LA-UR -85-158

Los Alamos National Laboratory is operated by the University of California for the United States Department of Energy under contract W-7405-ENG-36

LA-UR--85-158

DE85 005816

TITLE Slideline Verification for Multilayer Pressure Vessels and Piping Analysis Including Strain Hardening

AUTHOR(S) Leonard A. VanGulick (Collaborator, Group WX-11)

MASTER

SUBMITTED TO 1985 ASME Pressure Vessel and Piping Conference, New Orleans, LA

DISCLAIMER

Los Alamos Los Alamos National Laboratory
Los Alamos, New Mexico 87545

FORM NO 836 R4
ST NO 2629 5/81

SLIDELINE VERIFICATION FOR MULTILAYER PRESSURE VESSEL AND PIPING ANALYSIS INCLUDING STRAIN HARDENING

Leonard A. Van Gulick
Collaborator
Los Alamos National Laboratory
Los Alamos, New Mexico
Member ASME

Nonlinear finite element computer codes with slideline algorithm implementations are useful for the analysis of prestressed pressure vessels and piping. This paper presents closed form solutions including the effects of linear strain hardening useful for verifying slideline implementations for this application. The solutions describe stresses and displacements of an internally pressurized inner sphere initially separated from an outer sphere by a uniform gap. Linear strain hardening material behavior following yield for the inner sphere and elastic material behavior for the outer sphere are assumed. Comparison of closed form and finite element results evaluates the usefulness of the closed form solutions and the validity of the slideline implementation used.

NOMENCLATURE

a, b	inner and outer radii, inner sphere
c, d	inner and outer radii, outer sphere
C_1, C_2	boundary condition dependent constants
E_1, E_2	Young's modulus, inner, outer spheres
E_t	plastic tangent modulus, inner sphere
K_1, K_2	elastic stiffness parameters, inner sphere
K_{1P}, K_{2P}	plastic stiffness parameters, inner sphere
K_3	stiffness parameter, outer sphere
K_4, K_5	combined stiffness parameters
m	linear strain hardening parameter
p	internal pressure, inner sphere
p_4^*	maximum pressure for separation
p_I	interface pressure
r	radius
u	displacement, outer surface, inner sphere
β_1, β_2	thickness ratio, inner, outer spheres
Δp	internal pressure change
Δp_I	interface pressure change
μ_1, μ_2	Poisson's ratio, inner, outer spheres
σ_θ	hoop stress, inner sphere
σ_r	radial stress, inner sphere
$\sigma_\theta^e, \sigma_r^e$	elastic unloading stresses
σ_y	yield stress, inner sphere

Subscripts Denote Quantities Associated With:

1	initial yielding
2	complete yielding
3	gap closure
4	peak pressurization
5	separation
6	complete pressure release
7	operating conditions

INTRODUCTION

The development and implementation in nonlinear finite element method (FEM) computer codes of slideline algorithms (1) should facilitate the inclusion of the effects of initial interlayer gaps in the analysis of prestressed multilayer pressure vessels and piping (2). Verification of the ability of FEM codes to carry out this analysis has been limited, however, by a scarcity of appropriate closed form solutions to which code results could be compared. Needed are closed form solutions for stresses and displacements for problems that include initiation and termination of interlayer contact and plastic material behavior followed by elastic unloading and subsequent reloading.

Closed form solutions previously presented for slideline verification (3,4) assumed elastic-perfectly plastic material behavior. This paper presents closed form solutions that include linear strain hardening material behavior. The solutions make possible the verification of code ability to include strain hardening in prestressed multilayer pressure vessel analysis.

The problem treated consists of two concentric thick walled spheres subjected to internal pressure. The two spheres are initially separated by a uniform gap large enough to allow complete yielding of the inner sphere before it contacts the outer one. Linear strain hardening behavior for the inner sphere and elastic behavior for the outer sphere are assumed. A pressure-time history consisting of initial pressurization, pressure release, and repressurization to operating pressure is considered.

Closed form results for a particular choice of geometry and pressure levels are compared to FEM results obtained using ADINA(5) and a recently implemented slideline algorithm (6). The comparison leads to an evaluation of the value of the closed form solutions for slideline validation and of the validity of the particular slideline implementation used.

CLOSED FORM FORMULATION

Equations for the stresses and displacements in an elastic sphere subjected to internal and external pressures are readily available (7). Standard plasticity texts (8) describe the stresses and displacements in linear strain hardening spheres. These results can be extended and combined to develop solutions for the two spheres with inner and outer radii a , b and c , d , shown in Fig. 1.

The pressure-displacement diagram shown in Fig. 2 relates the displacement of the outer surface of the inner sphere to internal pressure during initial pressurization to peak pressure, p_4 , pressure release, and repressurization to operating pressure, p_7 . As shown, separation may or may not occur during pressure release, depending on the peak pressure chosen.

The slope of the preyield portion of the diagram is determined by the elastic stiffness, K_1 , of the inner sphere

$$K_1 = \frac{2 E_1 (\beta_1^3 - 1)}{3 b (1-\mu_1)} \tag{1}$$

where β_1 is the thickness ratio

$$\beta_1 = b/a \tag{2}$$

and E_1 and μ_1 are Young's modulus and Poisson's ratio for the inner sphere.

The pressure at which yielding begins, p_1 , and the corresponding displacement, u_1, are

$$p_1 = \frac{2 \sigma_y (\beta_1^3 - 1)}{3 \beta_1^3} \tag{3}$$

$$u_1 = \frac{b \sigma_y (1-\mu_1)}{\beta_1^3 E_1} \tag{4}$$

where σ_y is the yield stress for the inner sphere.

Yielding completely through the wall of the inner sphere occurs at pressure, p_2 , and produces displacement, u_2

$$p_2 = \left\{ \frac{(4/3)(1-\mu_1) m (\beta_1^3 - 1) + 2(1-m) \ln \beta_1}{2m(1-\mu_1) + (1-m)} \right\} \sigma_y \tag{5}$$

$$u_2 = \sigma_y (1-\mu_1) b / E_1 \tag{6}$$

where m is the strain hardening parameter, defined as the ratio of the plastic tangent modulus, E_t, to Young's modulus

$$m = E_t / E \tag{7}$$

The fully yielded strain hardening inner sphere continues to expand with increasing pressure until contact with the outer sphere occurs at 3. The slope of the diagram between 2 and 3 is determined by the plastic stiffness, K_{1P}, of the inner sphere

$$K_{1P} = \frac{4E_1(\beta_1^3-1)}{3b}\left(\frac{m}{1+m(1-2\mu_1)}\right) \tag{8}$$

Contact occurs when the displacement is equal to the initial gap

$$u_3 = c-b \tag{9}$$

The corresponding pressure, p_3, is given by

$$p_3 = p_2 + K_{1P}(u_3 - u_2) \tag{10}$$

The slope of the remainder of the loading curve is the combined stiffness, K_4, of the strain hardening inner sphere and elastic outer sphere

$$K_4 = K_{1P}(K_{2P}-K_3)/K_{2P} \tag{11}$$

where K_{2P} is a stiffness parameter relating displacement at the outer surface of the strain hardening inner sphere to external pressure at that surface

$$K_{2P} = -\frac{4E_1(\beta_1^3-1)}{c}\left(\frac{m}{3+(4\beta_1^3-1)m(1-2\mu_1)}\right) \tag{12}$$

and K_3 is a stiffness parameter relating displacement at the inner surface of the outer sphere to pressure at that surface.

$$K_3 = \frac{E_2}{c}\left[\frac{2(\beta_2^3-1)}{(1-\mu_2)(\beta_2^3+2)+2\mu_2(\beta_2^3-1)}\right] \tag{13}$$

The thickness ratio of the outer sphere is

$$\beta_2 = d/c \tag{14}$$

Maximum displacement, u_4, occurs at peak pressure p_4.

$$u_4 = u_3 + (p_4 - p_3)/K_4 \tag{15}$$

The two spheres unload elastically as an integral unit when pressure release begins. Their combined stiffness, K_5, determines the intial slope of the unloading curve

$$K_5 = K_1 (K_2 - K_3) / K_2 \qquad (16)$$

where K_2 is the stiffness parameter relating displacement at the outer suface of the elastic inner sphere to pressure acting on that surface.

$$K_2 = \frac{-2 E_1 (\beta_1^3 - 1)}{b((1+2\beta_1^3)(1-\mu_1) - 2\mu_1(\beta_1^3 - 1))} \qquad (17)$$

Separation will occur if the outer sphere reaches its undeformed position. The interface pressure acting at the boundary between the two spheres will then be zero and the inner sphere will move in alone with additional displacements related to further reductions in internal pressure by the original stiffness, K_1. The separation pressure, p_5,

$$p_5 = p_4 - K_5 (p_4 - p_3) / K_4 \qquad (18)$$

is physically meaningful only if positive. Negative values indicate complete pressure release without separation and are associated with peak pressures greater than p_4^*, the maximum peak pressure for which separation occurs.

$$p_4^* = K_5 p_3 / (K_5 - K_4) \qquad (19)$$

A residual displacement, u_6, exists when the initial pressure is fully released.

$$u_6 = u_3 - p_5 / K_1 \qquad p_4 \le p_4^* \qquad (20a)$$

$$u_6 = u_4 - p_4 / K_5 \qquad p_4 \ge p_4^* \qquad (20b)$$

Repressurization to operating pressure, p_7, produces elastic behavior described by proceeding back up along the unloading curve.

Radial and hoop stresses, σ_{4r} and $\sigma_{4\theta}$, at radius, r, in the inner sphere at peak pressure are given by

$$\sigma_{4r} = -p_4 + \frac{1}{(1+m(1-2\mu_1))}\left[2(1-m)\sigma_y \ln\left(\frac{r}{a}\right)\right. \qquad (21)$$

$$\left. + \frac{2m(1-\mu_1)\beta_1^3((r/a)^3 - 1)}{(\beta_1^3 - 1)(r/a)^3}\left\{(p_4 - p_{4I}) - \frac{(1-m)}{(1-\mu_1)m}\left(\sigma_y \ln(r/a) - \frac{(p_4 - p_{4I})}{2}\right)\right\}\right]$$

$$\sigma_{4\theta} = -p_4 + \frac{1}{(1+m(1-2\mu_1))}\left[(1-m)\sigma_y (1 + 2\ln(r/a))\right. \qquad (22)$$

$$\left. + \frac{2m(1-\mu_1)\beta_1^3((r/a)^3 + (1/2))}{(\beta_1^3 - 1)(r/a)^3}\left\{(p_4 - p_{4I}) - \frac{(1-m)}{(1-\mu_1)m}\left(\sigma_y \ln(r/a) - \frac{(p_4 - p_{4I})}{2}\right)\right\}\right]$$

where the maximum interface pressure, p_{4I} , is given by

$$p_{4I} = K_3(p_4 - p_3)/K_4 \tag{23}$$

Inner sphere stresses during pressure release are obtained by superimposing on the peak stresses a system of elastic stresses, σ_r^e and σ_θ^e ,

$$\sigma_r^e = \frac{2}{3}\left(1 - \frac{a^3}{r^3}\right) C_1 + \frac{C_2}{r^3} \tag{24}$$

$$\sigma_\theta^e = -\frac{1}{2}\sigma_r^e + C_1 \tag{25}$$

with constants C_1 and C_2 evaluated using boundary conditions

$$\sigma_r^e = -\Delta p \qquad r = a$$

$$\sigma_r^e = -\Delta p_I \qquad r = b$$

The changes in internal pressure and interface pressure, Δp and Δp_I , from peak pressures, p_4 and p_{4I} , will be negative during pressure release.

Residual stresses at complete pressure release

$$\Delta p = -p_4$$

are found using

$$\Delta p_I = -p_{4I}$$

when separation occurs and

$$\Delta p_I = -K_3 p_4 / K_5$$

when it does not.

$$\sigma_{6r} = \sigma_{4r} + \left(1 - \frac{a^3}{r^3}\right)\left(\frac{\beta_1^3}{\beta_1^3 - 1}\right)\left[\frac{K_3}{K_4}(p_4 - p_3) - \frac{p_4}{\beta_1^3}\right] + \frac{a^3}{r^3} p_4 \tag{26}$$

$$\sigma_{6\theta} = \sigma_{4\theta} + \frac{1}{2}\left(2 + \frac{a^3}{r^3}\right)\left(\frac{\beta_1^3}{\beta_1^3 - 1}\right)\left[\frac{K_3}{K_4}(p_4 - p_3) - \frac{p_4}{\beta_1^3}\right] - \frac{a^3}{2r^3} p_4 \tag{27}$$

$p_4 \leq p_4^*$ Separation Occurs

$$\sigma_{6r} = \sigma_{4r} + \left[\left(1 - \frac{a^3}{r^3}\right)\left(\frac{\beta_1^3}{\beta_1^3 - 1}\right)\left(\frac{K_3}{K_5} - \frac{1}{\beta_1^3}\right) + \frac{a^3}{r^3}\right] p_4 \qquad (28)$$

$$\sigma_{6\theta} = \sigma_{4\theta} + \frac{1}{2}\left[\left(2 + \frac{a^3}{r^3}\right)\left(\frac{\beta_1^3}{\beta_1^3 - 1}\right)\left(\frac{K_3}{K_5} - \frac{1}{\beta_1^3}\right) - \frac{a^3}{r^3}\right] p_4 \qquad (29)$$

$p_4 \geq p_4^*$ Separation Does Not Occur

Contact is assumed after repressurization to operating pressure, p_7 . The operating stresses, σ_{7r} and $\sigma_{7\theta}$, are found by adding the elastic stressses corresponding to

$$\Delta p = p_7 - p_4$$
$$\Delta p_I = K_3(p_7 - p_4)/K_5$$

to the stresses associated with peak pressure.

$$\sigma_{7r} = \sigma_{4r} + \left[\left(1 - \frac{a^3}{r^3}\right)\left(\frac{\beta_1^3}{\beta_1^3 - 1}\right)\left(\frac{K_3}{K_5} - \frac{1}{\beta_1^3}\right) + \frac{a^3}{r^3}\right](p_4 - p_7) \qquad (30)$$

$$\sigma_{7\theta} = \sigma_{4\theta} + \frac{1}{2}\left[\left(2 + \frac{a^3}{r^3}\right)\left(\frac{\beta_1^3}{\beta_1^3 - 1}\right)\left(\frac{K_3}{K_5} - \frac{1}{\beta_1^3}\right) - \frac{a^3}{r^3}\right](p_4 - p_7) \qquad (31)$$

FINITE ELEMENT METHOD CALCULATIONS

ADINA is a general purpose, nonlinear, finite element method structural analysis code into which a slideline algorithm that uses constraint equations based on the work of Taylor, Hughes, et al. (9) has been introduced. Contact compatibility is imposed by Lagrange multiplier techniques, with the multipliers representing nodal contact forces.

ADINA calculations were carried out for an arbitrarily chosen set of dimensions and material properties.

$$b/a = 1.25 \qquad c/a = 1.252 \qquad d/a = 1.50$$

$$E_1 = E_2 \qquad \mu_1 = \mu_2 \qquad \sigma_y = 1 \times 10^{-3} E_1$$

$$m = .1 \qquad p_4 = .8\sigma_y \qquad p_7 = .6\sigma_y$$

The axisymmetric finite element model used in the calculations is shown in Fig. 3. Symmetry considerations and the specification of zero meridonal displacements along radial boundries permitted consideration of only a 90° segment. The model has 902 node points and 800 four node elements. The contacting surfaces are each defined by 41 node points.

Calculations were carried out in a stepwise fashion because of the ADINA incremental solution scheme. A loading sequence of sixteen steps and an unloading sequence of twenty-four steps were used, with operating stresses determined during unloading. Much smaller steps were used in those portions of the calculations during which contact was initiated or terminated than were used elsewhere. No concerted effort was made to minimize the number of steps.

Equilibrium iteration was carried out at each load step and the stiffness matrix was reformulated as well. The Newton Raphson method was used to solve the incremental equilibrium equations. The ADINA material nonlinearity only analysis option was chosen because of the small displacements and strains associated with the subject problem. Averaging of Gauss point values to define element stresses was carried out as part of the postprocessing procedure. The inner sphere was modeled with ADINA material model eight, elastic- plastic with a von Mises yield criterion and isotropic hardening.

NUMERICAL RESULTS AND CONCLUSIONS

Distribut ons through the inner sphere wall of nondimensionalized peak, residual, and operating stresses are presented in Figs. 4 through 9. Excellent agreement is seen to exist between closed form and FEM results, even for residual stress calculations, which pose a severe test for slideline algorithms. Separation following pressure release is indicated by zero residual radial stress at the contact surface. This is an expected since the peak pressure, $.8\sigma_y$, is less than the maximum value for separation, $.97\sigma_y$.

The closed form results developed are seen to be useful for verifying FEM slideline implementations. They permit evaluation of implementation ability to correctly describe strain hardening material behavior in multilayer pressure vessels with initial interlayer gaps. The ADINA slideline implementation used can be considered as having been verified to correctly describe this type of behavior.

1. Hallquist, J. O., "A Numerical Treatment of Sliding Interfaces and Impact," AMD-Vol. 30, Computational Techniques for Interface Problems, Park, K. C. and Gartling, D. eds., American Society of Mechanical Engineers, 1978.

2. Uber, G. F. and Langford, P. J., "Analysis of Prestressed Double Wall Tubing for LMFBR Steam Generators," ASME Paper No. 81-PVP-25, American Society of Mechanical Engineers, 1981.

3. Van Gulick, L. A , "Slideline Verification for Multilayer Pressure Vessel and Piping Analysis," ASME Paper No. 83-PVP-28, American Society of Mechanical Engineers, 1983.

4. Van Gulick, L. A., "Slideline Verification for Multilayer Pressure Vessel and Piping Analysis Including Tangential Motion," ASME Paper No. 84-PVP-23, American Society of Mechanical Engineers, 1984.

5. Bathe, K. J., "Static and Dynamic Geometric and Material Nonlinear Analysis Using ADINA," Report 82448-2, Rev. 1977, M.I.T. Department of Mechanical Engineering, Acoustics and Vibrations Laboratory, Cambridge, Mass.

6. Guerra, F. M., and Browning, R. V., "Comparison of Two Slideline Algorithms Using ADINA," Computers and Structures, Vol. 17, Nos. 5-6, 1983, pp. 819-834.

7. Roark, R. H. and Young, W. C., Formulas for Stress and Strain, 5th ed., McGraw-Hill, New York, 1975, pp. 504- 506.

8. Mendelson, A., Plasticity: Theory and Application, 1st ed., Macmillan, New York, 1960, pp. 150-156.

9. Hughes, J. J. R. et al., "Finite Element Models for Large Displacement Contact-Impact Analysis," 76-4, July 1976, Department of Civil Engineering, University of California, Berkeley, California.

FIGURE 1

CONCENTRIC SPHERES

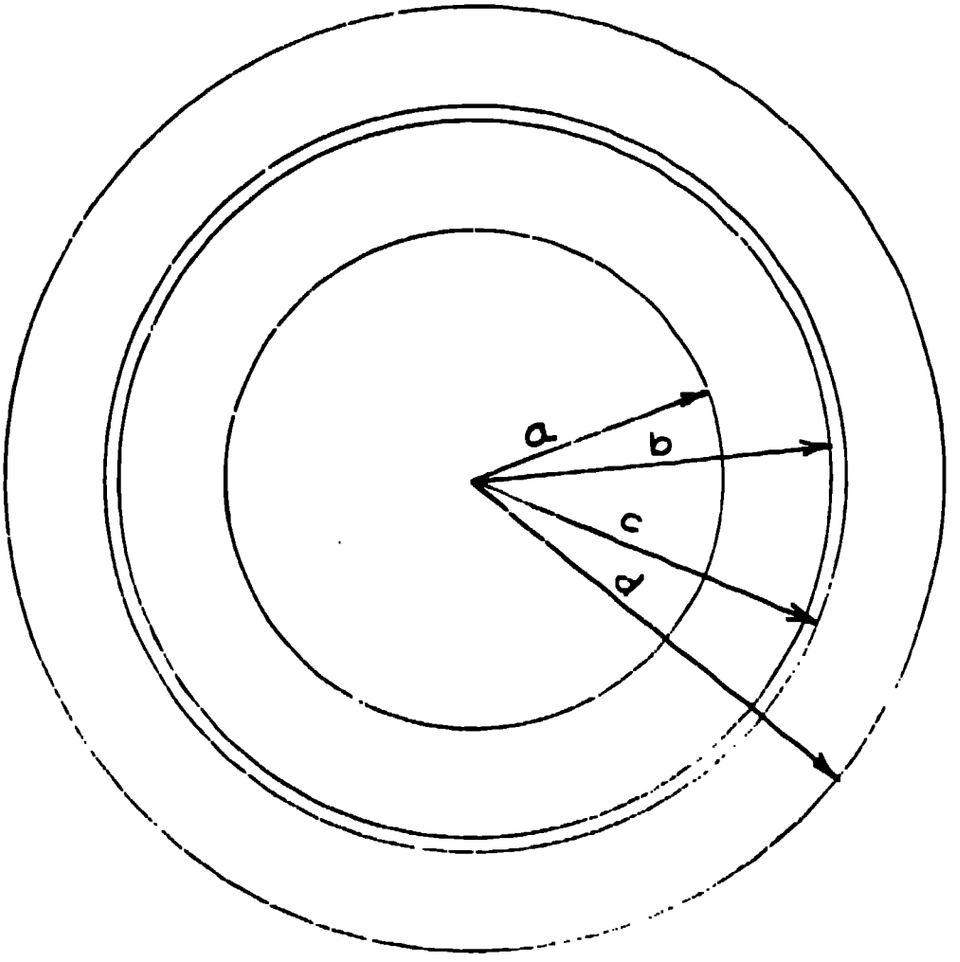

FIGURE 2

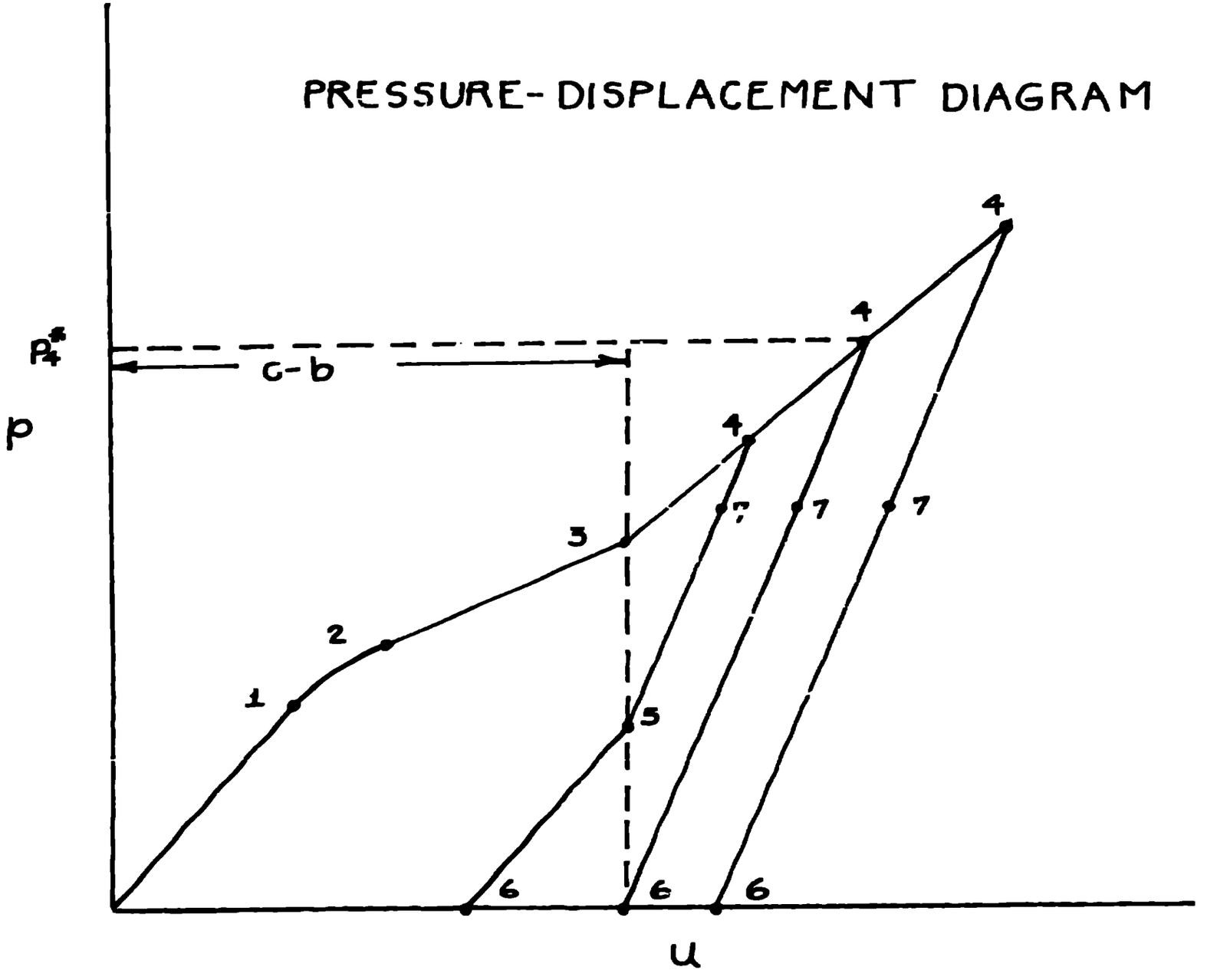

FIGURE 3

FINITE ELEMENT MODEL

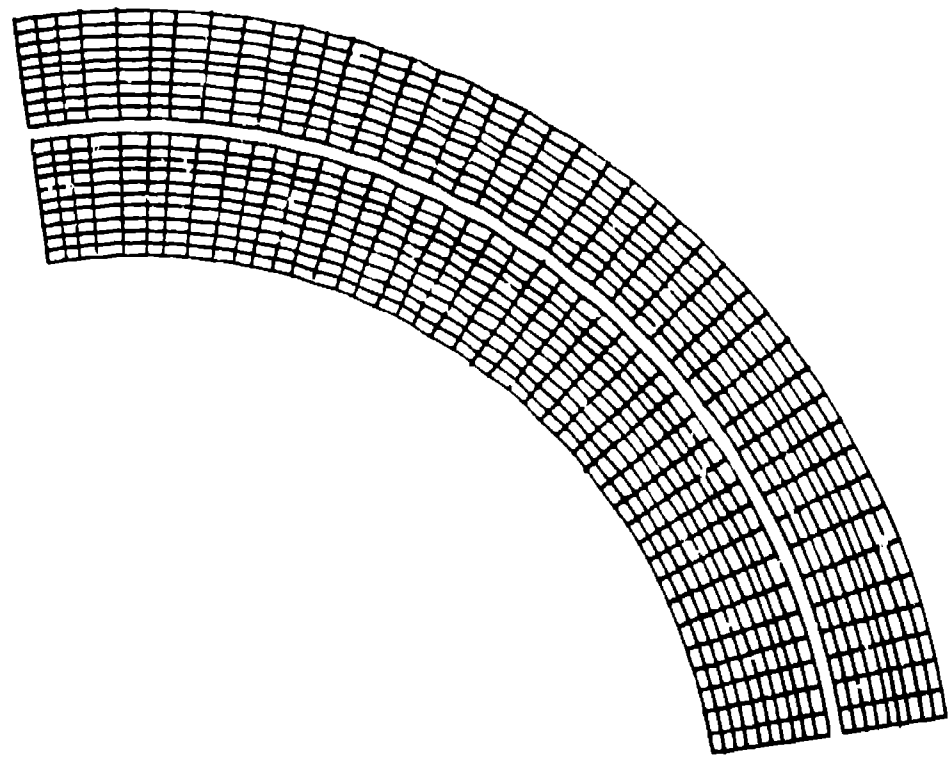

FIGURE 4

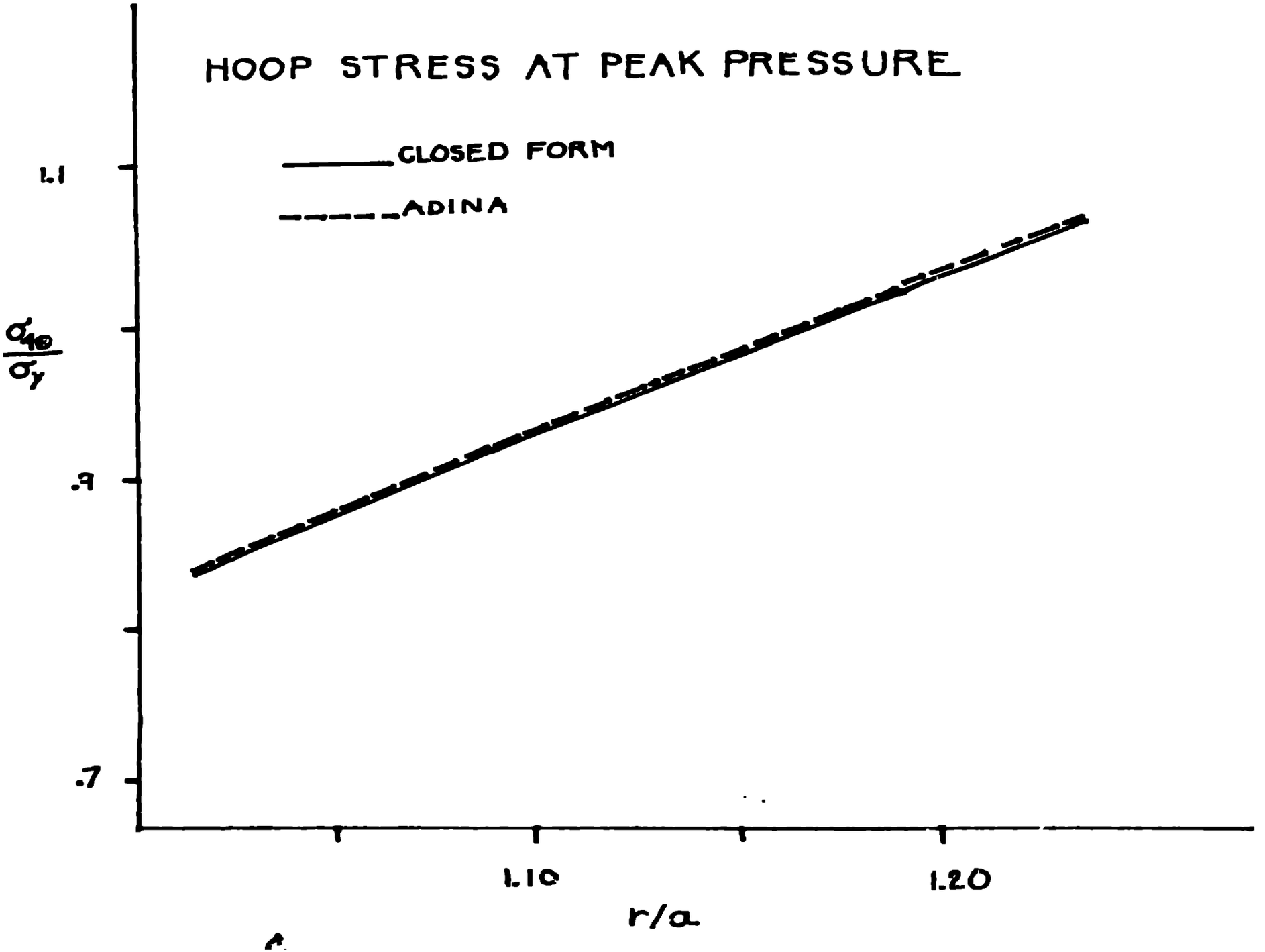
HOOP STRESS AT PEAK PRESSURE
CLOSED FORM
ADINA
1.1
.9
.7
$\frac{\sigma_{\theta\theta}}{\sigma_y}$
1.10
1.20
r/a

FIGURE 5

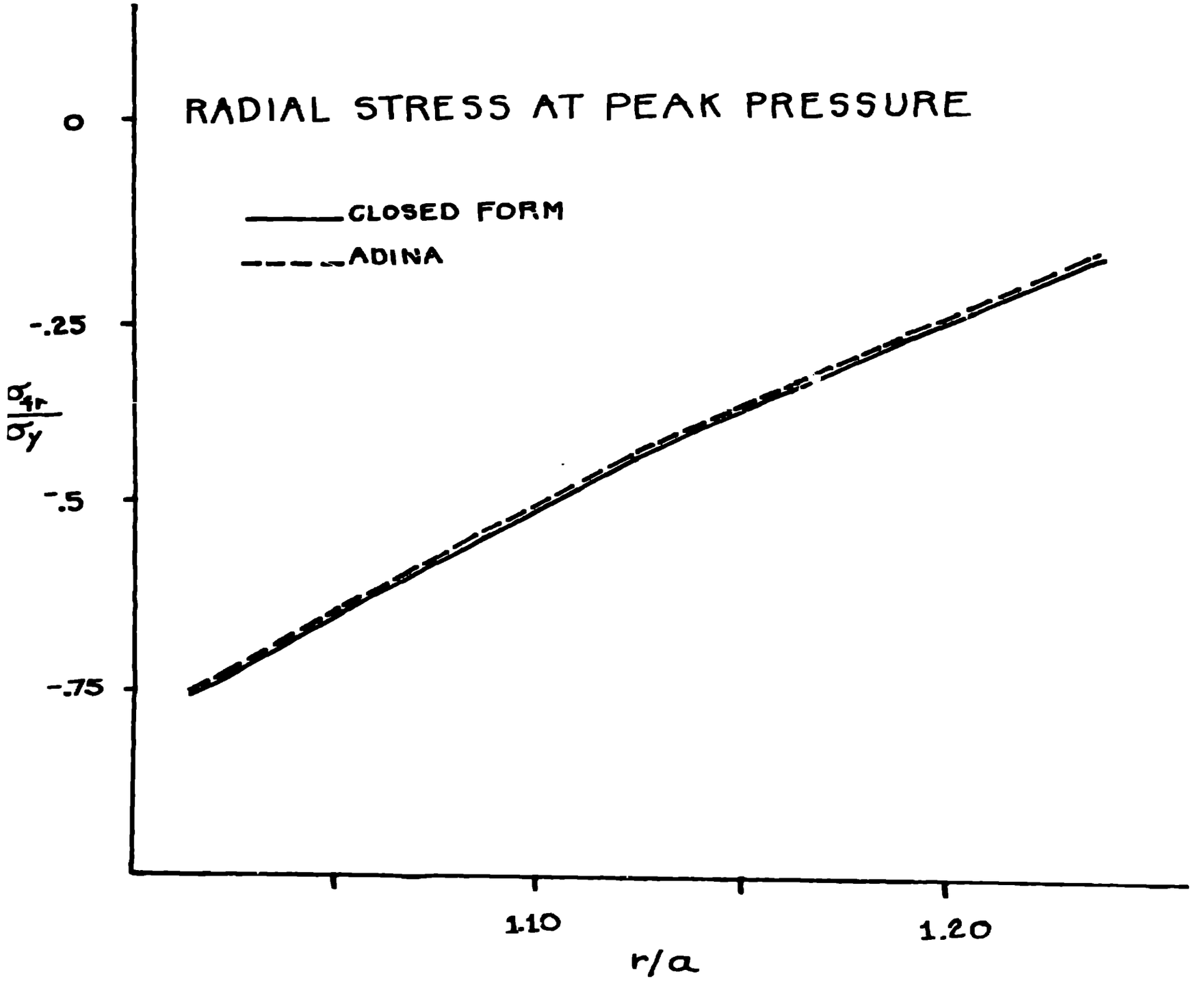
RADIAL STRESS AT PEAK PRESSURE
CLOSED FORM
ADINA
0
-.25
-.5
-.75
$\frac{\sigma_{4r}}{\sigma_y}$
1.10
1.20
r/a

FIGURE 6

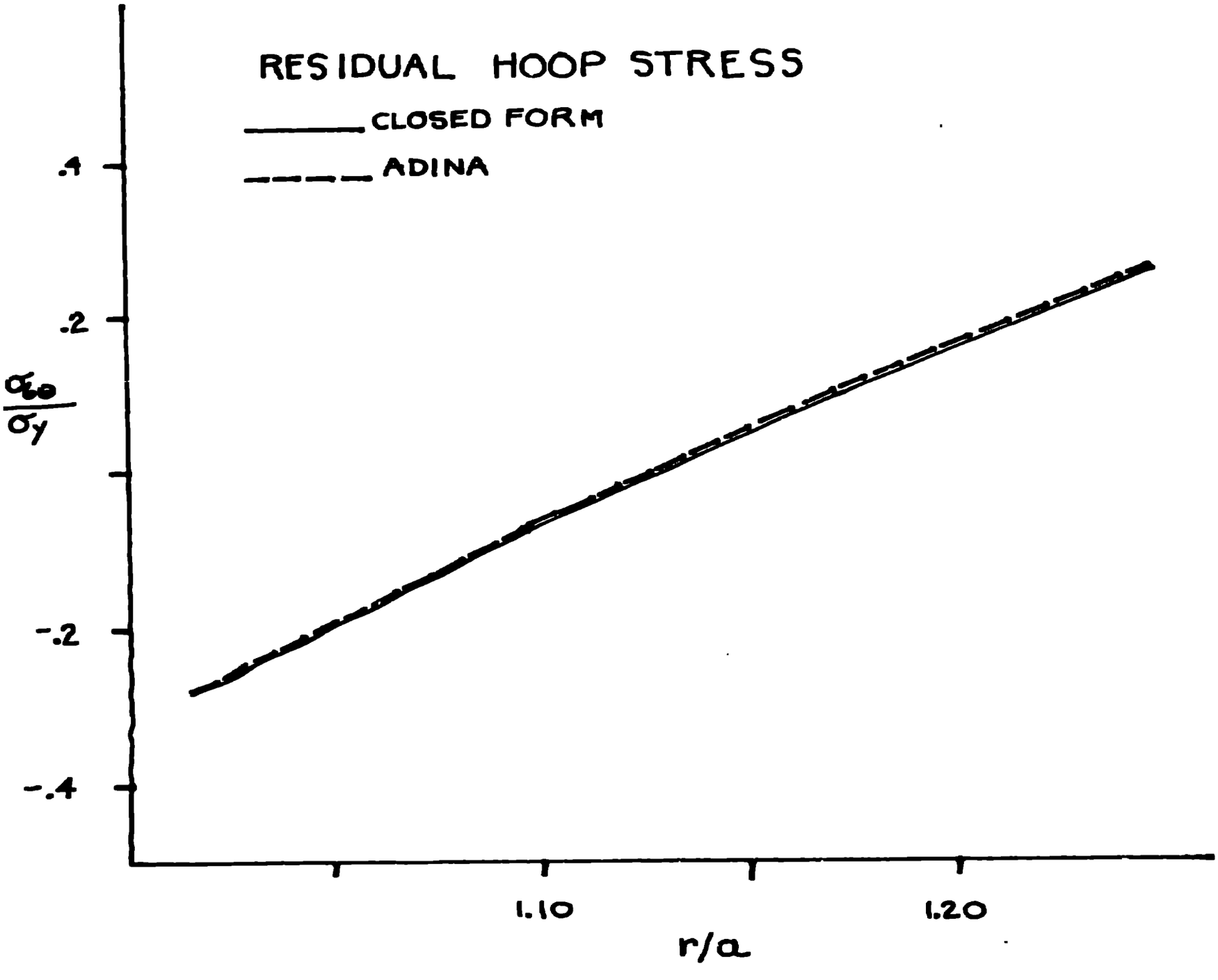
RESIDUAL HOOP STRESS
CLOSED FORM
ADINA
.4
.2
-.2
-.4
$\frac{\sigma_{\theta\theta}}{\sigma_y}$
1.10
1.20
r/a

FIGURE 7

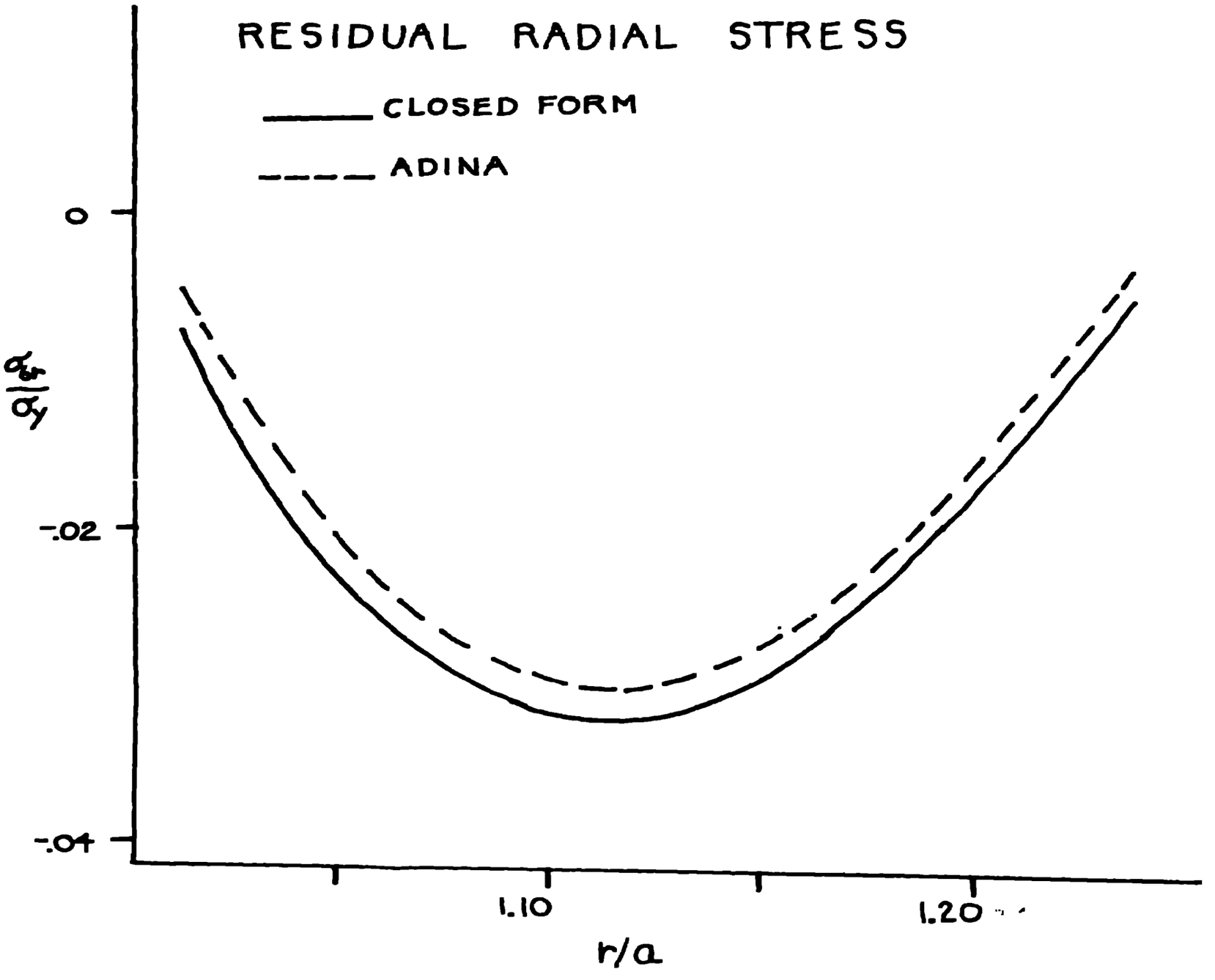
RESIDUAL RADIAL STRESS
CLOSED FORM
ADINA
0
-.02
-.04
σ_r/σ_r
1.10
1.20
r/a

FIGURE 8

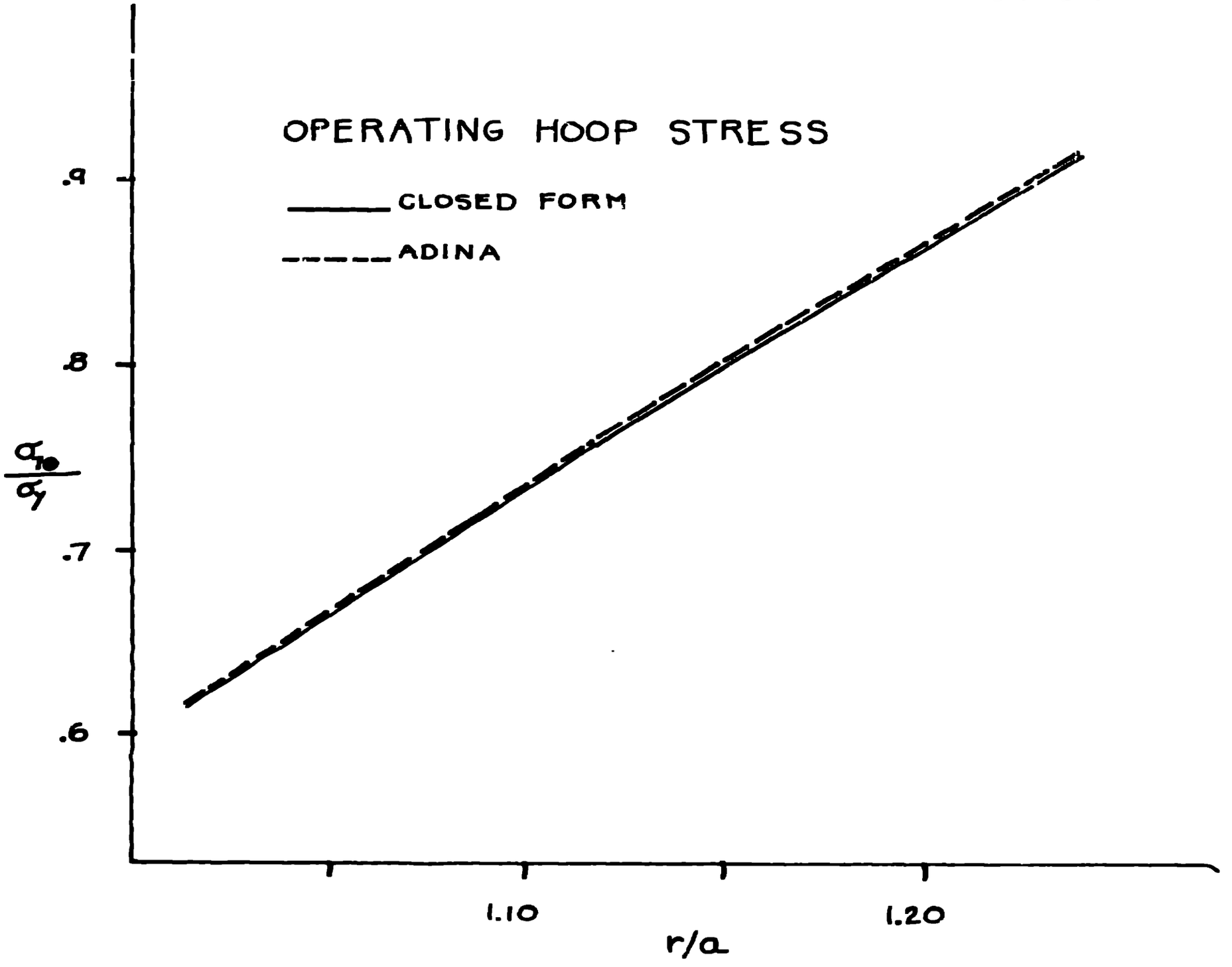
OPERATING HOOP STRESS
CLOSED FORM
ADINA
.9
.8
.7
.6
$\frac{\sigma_{\theta\theta}}{\sigma_y}$
1.10
1.20
r/a

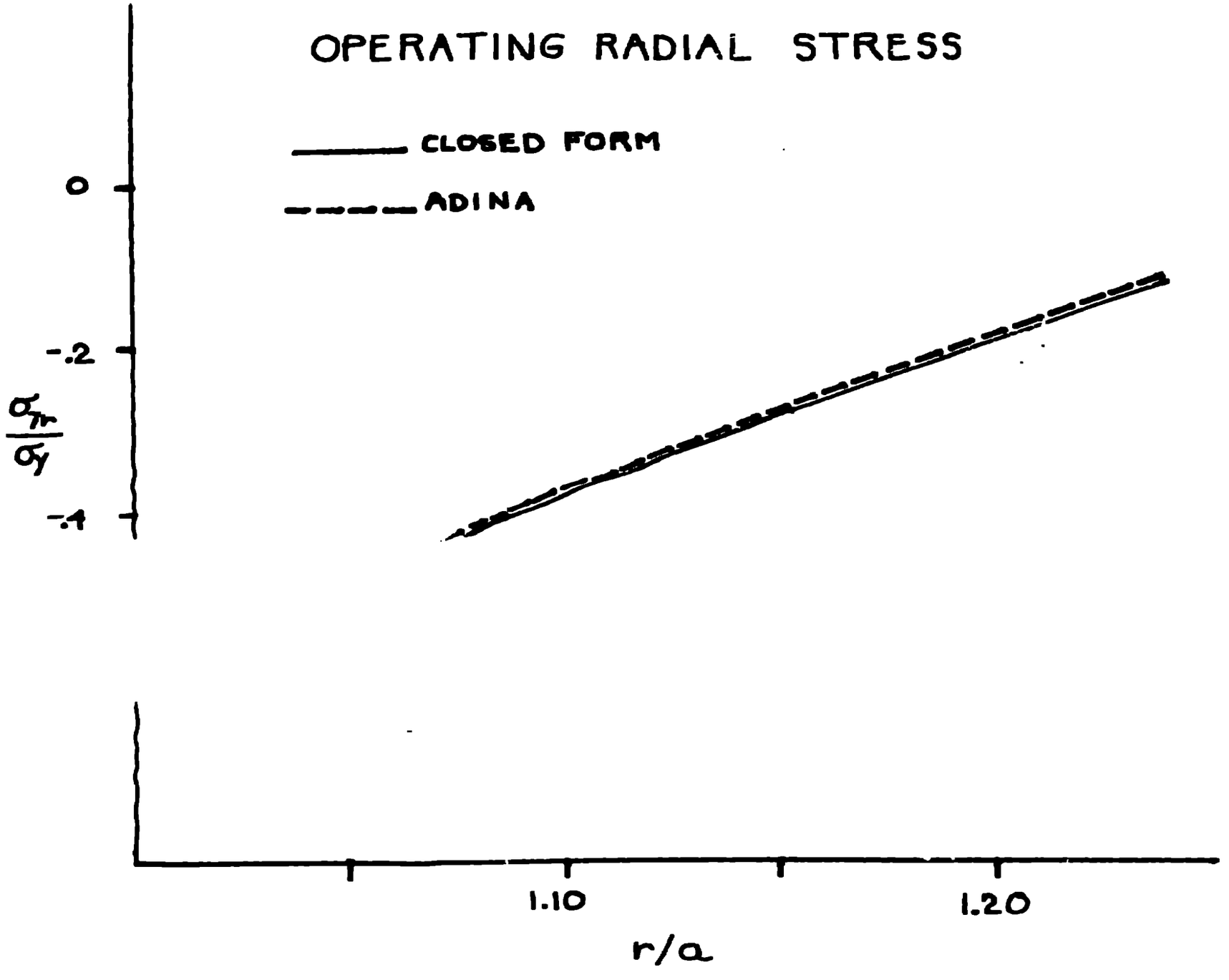
OPERATING RADIAL STRESS
CLOSED FORM
ADINA
0
-.2
-.4
$\frac{\sigma_r}{\sigma_y}$
1.10
1.20
r/a